Quaternary Science Reviews 149 (2016) 248–258

Contents lists available at ScienceDirect

Quaternary Science Reviews

journal homepage: www.elsevier.com/locate/quascirev

Quaternary evolution and ice sheet history of contrasting landscapes in Uummannaq and Sukkertoppen, western Greenland

C.R. Beel [a, *], N.A. Lifton [a, b], J.P. Briner [c], B.M. Goehring [d]

[a] Department of Earth, Atmospheric, and Planetary Sciences, Purdue University, 550 Stadium Mall Drive, West Lafayette, IN 47907, USA
[b] Department of Physics and Astronomy, Purdue University, 525 Northwestern Ave., West Lafayette, IN 47907, USA
[c] Department of Geology, State University of New York at Buffalo, Buffalo, NY 14260, USA
[d] Department of Earth and Environmental Sciences, Tulane University, 101 Blessey Hall, New Orleans, LA 70118, USA

A R T I C L E I N F O

Article history:
Received 5 February 2016
Received in revised form
18 May 2016
Accepted 20 May 2016

Keywords:
Cosmogenic nuclides
West Greenland
Greenland Ice Sheet
Landscape evolution
Quaternary

A B S T R A C T

Constraining the history of the Greenland Ice Sheet (GIS) is important for improving our understanding of ice sheet dynamics and landscape evolution processes. We analyzed *in situ* cosmogenic ^{10}Be and ^{26}Al in 26 rock samples from two high-elevation landscapes adjacent to the GIS, minimally eroded by past glaciations and of differing character in Uummannaq ($n = 16$) and Sukkertoppen ($n = 10$), western Greenland. The Uummannaq region is characterized by a marine embayment with islands and peninsulas, where the margin of the GIS is marine-based, whereas the Sukkertoppen landscape resides within the wide terrestrial fringe outboard of the land-terminating portion of the southwestern GIS margin. We targeted landscapes for sampling with highly weathered surfaces adjacent to cold-based portions of extant ice caps (indicated by preservation of fragile, dead vegetation emerging from beneath retreating ice margins). Paired isotope results require differing surface histories between the two areas. Many surfaces in the Uummannaq region have minimum exposure durations up to ca. 300 kyr, but with no significant burial. Most surfaces in the Sukkertoppen region, however, yield complex exposure histories with minimum cumulative exposure durations up to ca. 100 kyr and minimum cumulative burial durations up to ca. 400 kyr, yielding minimum total surface histories of up to 500 ka. These findings suggest that parts of the Uummannaq landscape may have been continuously exposed throughout much of the middle and late Quaternary. On the other hand, the high-altitude surfaces in the Sukkertoppen region were largely preserved beneath minimally-erosive, cold-based ice during the same period. Data from the Uummannaq region thus stand in contrast not only to the Sukkertoppen region, but also to other sites surrounding Baffin Bay reported in previous studies. We hypothesize that surfaces in the Uummannaq region may have remained as nunataks above the Last Glacial Maximum (LGM) ice sheet surface, as well as prior glacial maxima, due to significant ice surface drawdown by the Uummannaq Ice Stream System (UISS).

1. Introduction

The Greenland Ice Sheet (GIS) is undergoing rapid change in response to a warming climate (e.g., Seo et al., 2015). Because the GIS is one of the largest potential contributors to future sea-level change, understanding the longer-term GIS history is important for placing the present day changes in context (e.g., Lowell et al., 2013). A better understanding of the longer-term GIS history is also important to understanding its role in the global ocean-atmosphere-cryosphere system (e.g., Davis et al., 2006), for assessing the cryospheric expression of climate change (e.g., Briner et al., 2014), and improving our understanding of ice sheet dynamics (e.g., Corbett et al., 2011; Roberts et al., 2008, 2009; 2013; Lane et al., 2014). Furthermore, longer-term records of glacier history are important for understanding Quaternary landscape evolution at high latitudes (Gjermundsen et al., 2015).

Paired measurements of *in situ* cosmogenic ^{10}Be and ^{26}Al offer a robust approach for obtaining these longer-term glacial histories (Bierman et al., 1999). For example, in areas where ineffective glacial erosion has not completely eroded the cosmogenic nuclide

* Corresponding author. Department of Geography, Queen's University, Kingston, ON K7P 0C1, Canada.
E-mail address: 15cb29@queensu.ca (C.R. Beel).

http://dx.doi.org/10.1016/j.quascirev.2016.05.033
0277-3791/

inventory, paired measurements of the inherited ^{10}Be and ^{26}Al can be used to calculate a minimum sample history assuming one period of exposure followed by one period of burial in the Quaternary. These calculations allow inferences to be made about both long-term landscape evolution and glacial history (Gosse et al., 1995; Bierman et al., 1999; Fabel et al., 2002; Stroeven et al., 2002; Briner et al., 2006; Corbett et al., 2013, 2016).

Recent studies from polar landscapes have shown that upland surfaces are the product of multiple glacial-interglacial cycles, evolving over hundreds of thousands of years by episodic burial by minimally-erosive, cold-based ice (Bierman et al., 1999; Davis et al., 2006; Corbett et al., 2013; Briner et al., 2014). For example, high-elevation surfaces near Upernavik, western Greenland, record burial likely by cold-based ice for ca. 250–700 kyr of the last ca. 300–800 kyr (Corbett et al., 2013; values recalculated using procedures described below). This suggests that these surfaces have been preserved by repeated burial by glacial ice with little to no erosion for ca. 75–80% of their total history (Corbett et al., 2013). Similar results have also been found for uplands on Baffin Island, ca. 600 km to the west (e.g., Bierman et al., 1999; Briner et al., 2006). In contrast, two recent studies from the Uummannaq region, ca. 200 km south of Upernavik, found no significant burial in two bedrock samples from high-elevation inter-fjord plateaus, despite long exposure durations of ca. 85 and 120 kyr [recalculated data from Lane et al. (2014) and Roberts et al. (2013), respectively]. These findings suggest that the evolution of the landscape and the history of the GIS may vary for margins of differing character (e.g., glacial margins along marine embayment or terrestrial fringe settings).

To build on these findings, we compare the longer-term glacial history of the marine embayment setting of Uummannaq with that of the terrestrial fringe setting of the Sukkertoppen region (ca. 400 km to the south) along the western margin of the GIS (Fig. 1A). We present sixteen paired measurements of ^{10}Be and ^{26}Al concentrations from the Uummannaq region (Fig. 1B) and ten from the Sukkertoppen region (Fig. 1C). We targeted bedrock that exhibits signs of subaerial weathering on low-relief upland surfaces adjacent to cold-based portions of local ice caps separate from the GIS.

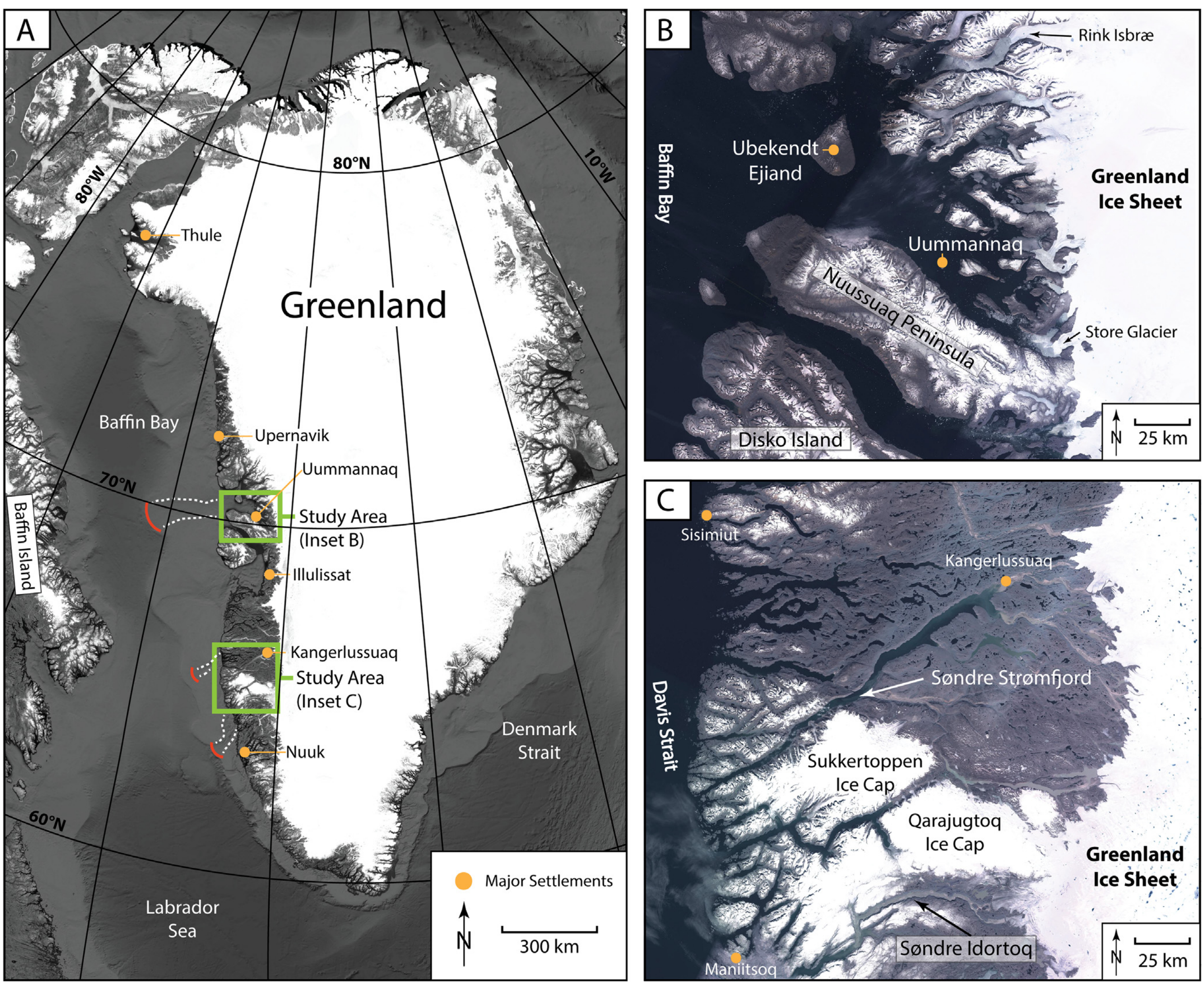

Fig. 1. A – Map of Greenland showing the study areas. B – the Uummannaq study region (marine embayment setting). C – the Sukkertoppen study region (terrestrial fringe setting). Major settlements and features are labeled. LGM ice stream systems in close proximity to our study areas indicated by dashed white lines. Maximum LGM extent on the outer shelf indicated by solid red lines. Note that the ice caps in our study areas are currently separate from the GIS, but were likely engulfed during GIS expansion. Ice caps are located on the relatively flat terrain of inter-fjord plateaus. Deep fjords are broadly oriented NW-SE in the Uummannaq region and NE-SW in the Sukkertoppen region (satellite image source: (a) Google Earth Pro – Google ©; Image © 2015 IBACO; Image © 2015 Landsat; Image © 2015 U.S. Geological Survey; (B; C) ASTER and SPOT-5 DEM's – Howat et al., 2014). (For interpretation of the references to colour in this figure legend, the reader is referred to the web version of this article.)

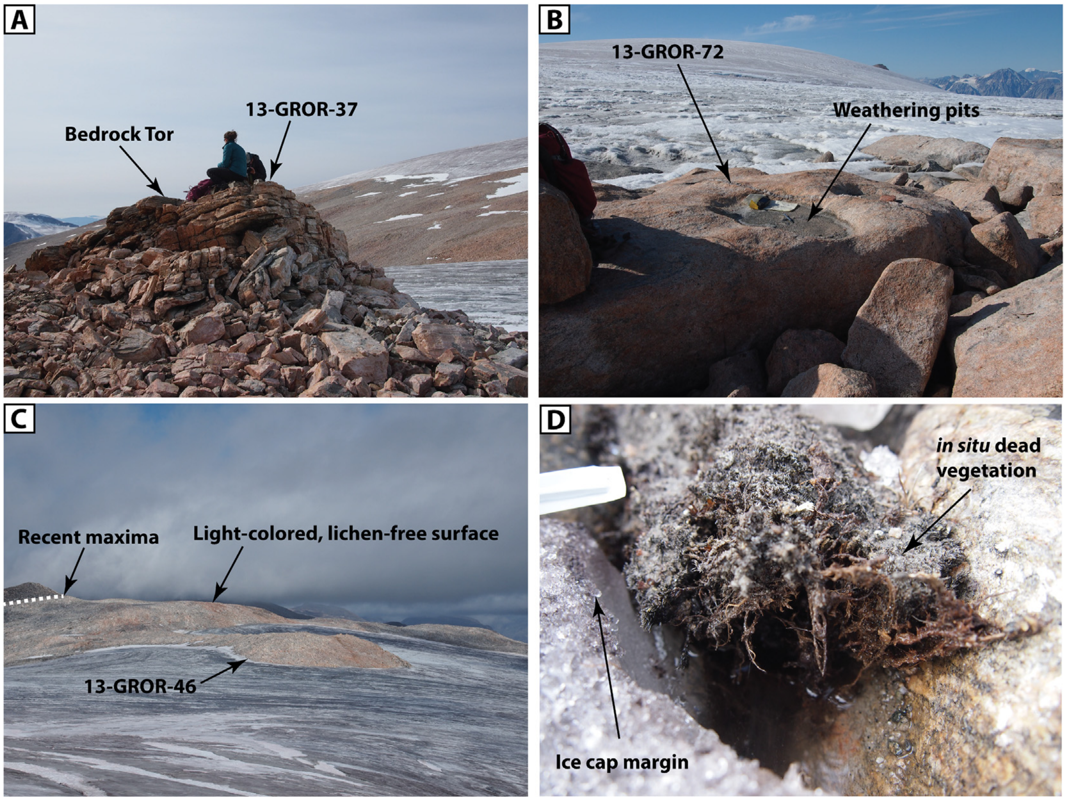

Fig. 2. Site photographs from the Uummannaq region. A – Sample 13-GROR-37 from atop a bedrock tor above autochthonous blockfield ca. 5 m from current ice margin and ca. 3 m above surrounding surface (to right of photo frame). B – Weathering pits with dimensions ca. 1.0 × 0.5 m, and up to 0.1 m deep, on an *in situ* blockfield slab within 2 m of existing ice cap margin. 13-GROR-72 collected from quartz-vein on top of blockfield slab. Note sample bag for scale. C – Looking north from 13-GROR-45 sample site toward 13-GROR-46. Note the position of the sample next to the existing ice cap margin, the relatively recent maxima extent of the ice cap (dashed line), and the light-colored lichen free surface. D – At all sites the presence of dead vegetation adjacent to sample sites indicates the preservation of surfaces beneath minimally-erosive, cold-based ice.

2. Study areas

2.1. Uummannaq region (marine embayment setting)

The Uummannaq region is located in central-west Greenland between ca. 70–72°N, ca. 50–55°W, with numerous local ice caps outboard of the western margin of the GIS (Fig. 1B). Our research area extends from the southern portion of the Nuussuaq Peninsula to the uplands in the south-central Uummannaq Fjord system. This high-relief area (>2 km) is highly dissected by a series of large fjords, that trend generally from southeast to northwest (Roberts et al., 2013). During glaciations, these fjords route ice streams from the GIS out onto the continental shelf (Roberts et al., 2013; Lane et al., 2014). At present, only fjord heads are occupied by marine-terminating outlet glaciers, draining the western GIS.

Inter-fjord plateaus in the Uummannaq area are presently occupied by local ice caps, ranging in elevation from 650 to 1300 m asl. Exposed surfaces include abundant weathered bedrock tors (Fig. 2A) and autochthonous blockfield slabs with weathering pits of varying dimensions (Fig. 2B); there is a general lack of glacial sculpting. Bedrock geology of the Uummannaq region is dominated by a Precambrian crystalline basement (primarily banded gneisses), overlain by Paleocene basaltic flows to the west of the region (Chalmers et al., 1999). A fault-bounded Cretaceous-Tertiary sedimentary basin also overlies the center of the Uummannaq region (Roberts et al., 2013; Lane et al., 2014).

2.2. Sukkertoppen region (terrestrial fringe setting)

The Sukkertoppen region is located between ca. 65–66°N, ca. 50–52°W, ca. 400 km south of the Uummannaq region (Fig. 1C). A wide terrestrial fringe separates the coastline of Baffin Bay and the Labrador Sea from the GIS, ca. 200 km to the east. In this area we focused on weathered bedrock surfaces exposed at the retreating cold-based margins of the two largest ice caps – the Sukkertoppen Ice Cap and the Qarajugtoq Ice Cap (both ca. 2000 km^2) (Weidick et al., 1992; Kelly and Lowell, 2009). Preserved along the retreating edges of the ice cap fringes is rooted surface moss, patterned ground and weathered bedrock attesting to the non-erosive nature of ice caps in our study sites. Ice caps in this study area rest atop large, relatively flat plateaus that are dissected to the north by the Søndre Strømfjord and to the south by Søndre Idortoq (Fig. 1C) (Kelly and Lowell, 2009). These widely spaced fjords route inland ice streams to the coast and out onto the continental shelf during expansion of the GIS (Roberts et al., 2009, 2010).

Similar to the Uummannaq region, exposed surfaces include weathered bedrock tors (Fig. 3A), and surfaces with weathering pits of varying dimensions (Fig. 3B and C). The presence of highly weathered bedrock along retreating ice cap margins confirm that our collection sites were covered by cold-based ice (e.g., Lowell et al., 2013; Miller et al., 2013a, 2013b). Precambrian gneisses and granitic rocks dominate the regional geology of this area (Henriksen, 2008).

3. Methods

3.1. Field sampling procedures

Quartz-bearing rock samples for ^{10}Be and ^{26}Al measurements were collected from the Uummannaq region in 2013 and from the

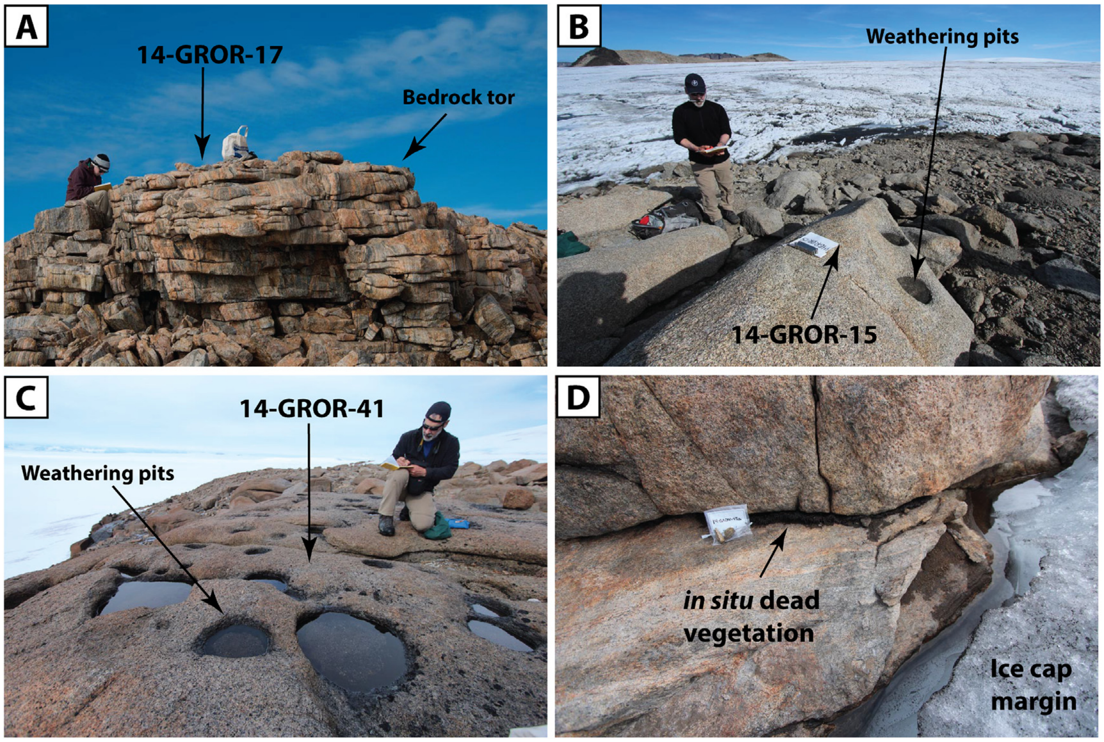

Fig. 3. Site photographs from the Sukkertoppen region. A – Sample 14-GROR-17 from atop a highly weathered bedrock tor above the surrounding ice surface along the northern extent of the Sukkertoppen Ice Cap. B – Sample 14-GROR-15 from a small ice cap disconnected from the main Sukkertoppen Ice Cap. Note large weathering pits on the sampled surface. C – Sample 14-GROR-41 from a highly weathered bedrock nunatak. Note extensive weathering pits of varying size on the bedrock surface. Note person for scale in all sample photographs. D – At all sites the presence of dead vegetation adjacent to sample sites indicates the preservation of surfaces beneath minimally-erosive, cold-based ice.

Table 1
Sample information and ^{10}Be and ^{26}Al measurement data.

Sample	Latitude (°N)	Longitude (°W)	Elevation (m asl)	Thickness (cm)	Quartz (g)	^{9}Be carrier (g)	^{10}Be/^{9}Be (10^{-15})	Total Al[f] (mg)	^{26}Al/^{27}Al (10^{-15})
Central-west Greenland: *Nuussuaq Peninsula*									
13-GROR-36[c]	70.26325	−52.11523	1110	1.5	30.048	0.6075	1146.9 ± 27.8	2.500 ± 0.0180	1517.0 ± 30.2
13-GROR-37[a]	70.25188	−51.81264	1248	3.0	31.697	0.7620	2030.0 ± 30.0	3.411 ± 0.0175	2189.7 ± 41.7
13-GROR-39[c]	70.22749	−52.06298	1231	1.0	30.095	0.6499	2030.5 ± 30.8	2.187 ± 0.0239	3073.0 ± 74.4
13-GROR-45[c]	70.20472	−51.06896	938	2.0	30.354	0.6009	725.8 ± 14.9	2.496 ± 0.0224	892.1 ± 21.8
13-GROR-46[b]	70.21574	−51.07764	864	2.0	33.249	0.9294	404.8 ± 13.1	0.507 ± 0.0109	4197.6 ± 213.7
13-GROR-57[c]	70.35495	−51.49591	1360	2.0	30.051	0.6354	3879.3 ± 61.1	2.337 ± 0.0172	5389.1 ± 76.3
13-GROR-58[c]	70.34951	−51.24879	1051	5.0	30.095	0.6271	411.3 ± 11.0	10.062 ± 0.0558	132.7 ± 7.4
13-GROR-59[c]	70.35273	−51.23903	1026	5.0	30.047	0.5400	1771.7 ± 38.9	10.237 ± 0.0698	492.5 ± 15.8
13-GROR-61[b]	70.33316	−51.36342	1200	5.0	30.328	0.7567	1437.7 ± 28.9	1.720 ± 0.0068	3533.6 ± 197.7
13-GROR-63[e]	70.32828	−51.36302	1183	4.5	33.998	0.7777	396.5 ± 6.9	2.498 ± 0.0222	2327.5 ± 49.8
13-GROR-64[b]	70.32256	−51.36193	1147	2.0	30.112	0.9328	747.6 ± 26.0	0.569 ± 0.0098	6762.7 ± 378.2
13-GROR-65[b]	70.32146	−51.37557	1190	2.5	29.490	0.5557	394.4 ± 15.7	0.434 ± 0.0093	3085.3 ± 103.8
Central-west Greenland: *Uummannaq Fjord*									
13-GROR-69[b]	70.68753	−51.82554	1184	2.0	29.884	0.9192	1625.3 ± 56.3	0.838 ± 0.0133	10954.3 ± 259.6
13-GROR-70[b]	70.90289	−52.05151	1497	2.0	30.068	0.6697	11422.1 ± 170	0.663 ± 0.0101	62170.9 ± 1948.2
13-GROR-71[a]	71.00298	−51.69919	1404	2.0	30.239	0.7643	9940.0 ± 120	3.543 ± 0.0387	11511.0 ± 138.4
13-GROR-72[a]	70.97373	−51.42089	1208	2.0	29.727	0.7666	6170.0 ± 110	3.900 ± 0.0280	6068.2 ± 104.2
South-west Greenland: *Sukkertoppen Ice Cap*									
14-GROR-02[d]	65.69620	−51.38621	988	2.5	30.125	0.7725	154.4 ± 3.5	2.897 ± 0.0185	698.4 ± 22.0
14-GROR-03[d]	65.93228	−51.50253	1162	2.5	30.412	0.7751	305.2 ± 6.4	2.969 ± 0.0141	1552.4 ± 36.7
14-GROR-14[d]	66.29550	−52.60647	1406	2.5	30.734	0.7771	318.3 ± 5.5	6.184 ± 0.0438	923.8 ± 41.7
14-GROR-15[d]	66.29484	−52.60547	1399	3.0	30.750	0.7483	448.0 ± 7.6	3.795 ± 0.0190	1669.0 ± 43.0
14-GROR-16[d]	66.37012	−52.76334	1558	2.0	30.882	0.7748	1089.9 ± 16.4	3.265 ± 0.0265	4927.4 ± 91.4
14-GROR-17[d]	66.33124	−52.42447	1598	6.5	30.214	0.7726	539.1 ± 8.1	3.001 ± 0.0254	2320.6 ± 47.9
14-GROR-39[e]	65.95237	−51.01990	1545	4.0	30.056	0.7779	529.8 ± 8.7	2.147 ± 0.0271	3259.2 ± 62.0
14-GROR-40[e]	65.95242	−51.01829	1550	1.0	30.563	0.6982	559.2 ± 12.9	2.481 ± 0.0197	2627.0 ± 131.7
14-GROR-41[e]	65.97914	−51.07040	1613	4.0	31.069	0.7823	876.2 ± 12.1	2.124 ± 0.0210	5515.3 ± 100.7
14-GROR-43[e]	66.06223	−51.65926	1350	1.5	30.183	0.7797	524.4 ± 8.9	2.407 ± 0.0217	3888.0 ± 248.4

Notes: All shielding correction factors were 1.000 except for 13-GROR-37 (0.957), 13-GROR-58 (0.997), and 14-GROR-40 (0.999). Al blank data summarized in the Supplementary Material. All quoted uncertainties are at the 1σ level, unless otherwise stated.

[a] 13-GROR-37, -71, -72 samples – Blank of $9.046 \pm 2.586 \times 10^{4}$ at g^{-1} carrier (0.7674 g, 280 ppm Be Carrier (supplied by John Gosse, Dalhousie University), $6.30 \pm 1.80 \times 10^{-15}$ ^{10}Be/^{9}Be).

[b] 13-GROR-46, -61, -64, -65, -69, -70 samples – Blank of $4.599 \pm 1.193 \times 10^{4}$ at g^{-1} carrier (0.8166 g, 280 ppm Be Gosse Carrier, $3.01 \pm 0.78 \times 10^{-15}$ ^{10}Be/^{9}Be).

[c] 13-GROR-36, -39, -45, -57, -58, -59 samples – Blank of $6.716 \pm 1.590 \times 10^{4}$ at g^{-1} carrier (0.4937 g, 280 ppm Be Gosse Carrier, $7.27 \pm 1.72 \times 10^{-15}$ ^{10}Be/^{9}Be).

[d] 14-GROR-02, -03, -14, -15, -16, -17 samples – Blank of $2.541 \pm 1.137 \times 10^{4}$ at g^{-1} carrier (0.7713 g, 1041 ppm Be, 2014.10.20-Be Carrier, $1.04 \pm 0.38 \times 10^{-15}$ ^{10}Be/^{9}Be).

[e] 13-GROR-63, 14-GROR-39, -40, -41, 43 samples – Blank of $5.605 \pm 2.060 \times 10^{4}$ at g^{-1} carrier (0.7818 g, 1041 ppm Be, 2014.10.20-Be Carrier, $0.47 \pm 0.21 \times 10^{-15}$ ^{10}Be/^{9}Be).

[f] Total Al analyzed using Inductively Coupled Plasma – Optical Emission Spectroscopy (ICP-OES).

Table 2
^{10}Be and ^{26}Al analytical and Monte Carlo exposure/burial results.

Nuclide Concentrations				*Site Production Rates*			*Monte Carlo Modeling*		
Sample	^{10}Be (10^5 at g^{-1})	^{26}Al (10^6 at g^{-1})	$^{26}Al/^{10}Be$ ratio	Minimum detectable burial (ky)	^{10}Be (at g^{-1} y^{-1})	^{26}Al (at g^{-1} y^{-1})	Minimum exposure (ky)	Minimum burial (ky)	Minimum total history (ky)
Central-west Greenland: Nuussuaq Peninsula									
13-GROR-36	4.316 ± 0.138	2.814 ± 0.056	6.50 ± 0.22	146	12.31	82.24	36.7 ± 2.3	–	–
13-GROR-37	9.102 ± 0.163	5.259 ± 0.100	5.78 ± 0.15	111	13.12	87.57	83.3 ± 3.6	270.3 ± 55.8	353.6 ± 55.9
13-GROR-39	8.182 ± 0.149	4.980 ± 0.121	6.09 ± 0.18	127	13.75	91.76	66.5 ± 3.1	167.5 ± 63.6	234.0 ± 63.7
13-GROR-45	2.666 ± 0.062	1.634 ± 0.041	6.10 ± 0.21	149	10.45	69.93	28.8 ± 1.6	185.8 ± 73.2	214.6 ± 73.2
13-GROR-46	2.103 ± 0.072	1.427 ± 0.073	6.81 ± 0.42	273	9.63	64.52	21.8 ± 2.0	–	-*
13-GROR-57	15.32 ± 0.286	9.350 ± 0.132	6.11 ± 0.14	98	15.21	101.45	113.0 ± 4.7	–	–
13-GROR-58	1.581 ± 0.046	0.987 ± 0.056	6.25 ± 0.39	278	11.29	75.52	15.8 ± 1.4	–	–
13-GROR-59	5.935 ± 0.144	3.741 ± 0.120	6.30 ± 0.25	171	11.06	73.95	60.0 ± 3.6	–	–
13-GROR-61	6.697 ± 0.151	4.472 ± 0.250	6.67 ± 0.40	266	12.38	82.64	56.7 ± 4.3	–	–
13-GROR-63	6.293 ± 0.127	3.814 ± 0.083	6.05 ± 0.18	129	12.76	85.24	57.4 ± 2.7	189.8 ± 61.2	247.2 ± 61.2
13-GROR-64	4.318 ± 0.157	2.854 ± 0.160	6.60 ± 0.44	297	11.6	77.49	38.5 ± 3.7	–	–
13-GROR-65	1.375 ± 0.057	1.014 ± 0.034	7.32 ± 0.39	235	12.93	86.19	9.8 ± 0.9	–	–
Central-west Greenland: Uummannaq Fjord									
13-GROR-69	9.338 ± 0.338	6.856 ± 0.163	7.34 ± 0.32	189	12.73	85.03	67.1 ± 5.3	–	–
13-GROR-70	47.758 ± 0.856	30.604 ± 0.959	6.43 ± 0.23	155	16.82	112.02	300.3 ± 14.4	–	–
13-GROR-71	46.977 ± 0.737	30.101 ± 0.362	6.40 ± 0.13	87	15.52	103.46	323.0 ± 11.2	–	–
13-GROR-72	29.740 ± 0.609	17.769 ± 0.305	5.99 ± 0.16	113	13.08	87.34	260.7 ± 12.7	–	–
South-west Greenland: Sukkertoppen									
14-GROR-02	2.747 ± 0.068	1.488 ± 0.050	5.44 ± 0.23	185	10.99	73.53	32.2 ± 2.0	440.3 ± 87.1	472.5 ± 87.1
14-GROR-03	5.403 ± 0.125	3.407 ± 0.083	6.33 ± 0.21	142	12.81	85.6	45.7 ± 2.5	–	–
14-GROR-14	5.590 ± 0.115	4.223 ± 0.192	7.56 ± 0.38	221	15.88	105.83	31.2 ± 2.0	–	–
14-GROR-15	7.575 ± 0.150	4.597 ± 0.120	6.08 ± 0.20	142	15.72	104.76	54.7 ± 2.7	172.5 ± 66.5	227.2 ± 66.6
14-GROR-16	19.56 ± 0.035	11.61 ± 0.216	5.92 ± 0.15	109	18.13	120.64	125.2 ± 5.2	192.5 ± 52.0	317.7 ± 52.2
14-GROR-17	9.121 ± 0.164	5.128 ± 0.106	5.63 ± 0.15	113	18.04	120.05	62.2 ± 2.7	332.5 ± 54.4	394.7 ± 54.5
14-GROR-39	9.520 ± 0.183	5.192 ± 0.100	5.45 ± 0.15	118	17.54	116.76	70.4 ± 3.1	404.2 ± 56.2	474.6 ± 56.3
14-GROR-40	8.868 ± 0.223	4.756 ± 0.239	5.36 ± 0.30	247	18.05	120.12	63.1 ± 4.9	437.5 ± 122.3	500.6 ± 122.4
14-GROR-41	15.328 ± 0.261	8.411 ± 0.154	5.50 ± 0.14	109	18.57	123.52	105.7 ± 4.3	336.5 ± 51.7	442.2 ± 51.9
14-GROR-43	9.404 ± 0.185	6.916 ± 0.442	7.35 ± 0.49	297	15.22	101.52	56.4 ± 4.7	–	–

Notes: Process blanks subtracted from concentrations. All samples were corrected for topographic shielding and sample thickness. No corrections were applied for transient snow cover, surface erosion, or local isostatic rebound. Assumed rock density 2.7 g cm^{-3}. Ratios of site production rates for $^{26}Al/^{10}Be$ differ from the canonical 6.75 at sea level and high latitude due to the use of nuclide-specific scaling per Lifton et al. (2014). Minimum exposure and burial durations, and the uncertainties associated with each, were calculated as the arithmetic mean and standard deviation of the 1000 Monte Carlo simulations. Analytical uncertainties, excluding those on production rates, are propagated through all calculations. All quoted uncertainties are at the 1σ level, unless otherwise stated. Dashes represent samples with indeterminate burial durations (i.e., continuous exposure). These were removed from analysis of burial durations as they yielded zero burial or unrealistic estimates (e.g., negative burial).

Sukkertoppen region in 2014. Bedrock and weathered blockfield (felsenmeer) slabs and tors were sampled from upland surfaces adjacent to contemporary cold-based portions of local ice caps. We targeted these areas because they provide the greatest likelihood of having surfaces that may have existed through multiple glacial-interglacial cycles. Samples were collected with hammer and chisel in 2013, and with a battery-powered angle grinder and hammer and chisel in 2014. We sampled sub-horizontal surfaces, away from edges and corners. Latitude, longitude, elevation, surface dip and dip direction, and topographic shielding measurements were recorded at each site. Sample altitudes ranged from 864 to 1497 m in the Uummannaq region and 988–1612 m in the Sukkertoppen region. Pertinent sample data are provided in Table 1.

3.2. Laboratory procedures

Samples were processed at the Purdue Rare Isotope Measurement (PRIME) Laboratory. Sample thicknesses were measured prior to crushing. Samples were crushed and sieved to separate the 250–500 μm size fraction. Quartz was isolated from this size fraction following standard procedures modified from Kohl and Nishiizumi (1992) (http://science.purdue.edu/primelab/labs/mineral-separation-lab/procedure.php). The samples were spiked with a known amount of ^{9}Be and dissolved in a mixture of hydrofluoric and nitic acid. Aluminum concentrations were determined using inductively coupled plasma optical emission spectrometry (ICP-OES). Be and Al were isolated using standard cation/anion exchange column procedures (Ochs and Ivy-Ochs, 1997). Hydroxides were calcined to BeO and Al_2O_3, mixed with Nb and Ag powders, respectively, and pressed into target holders for analysis by accelerator mass spectrometry (AMS) at PRIME Laboratory. $^{10}Be/^{9}Be$ ratios were normalized to the material 07KNSTD with a reported value of 2.85×10^{-12}, using a ^{10}Be half-life of 1.39×10^6 yr (Nishiizumi et al., 2007; Chmeleff et al., 2010; Korschinek et al., 2010). Normalizing with the ^{10}Be half-life used by Nishiizumi et al. (2007) (1.36×10^6 yr) does not affect the measured ratios significantly (<ca. 3‰). $^{26}Al/^{27}Al$ ratios were measured relative to standard KNSTD prepared by Nishiizumi (2004), with a reported value of 4.694×10^{-12}, and a ^{26}Al half-life of 7.05×10^5 yr. The total number of atoms in process blanks was subtracted from measured sample concentrations (Table 2). Process blank data for Be and Al are summarized in Table 1 and the Supplementary Material, respectively.

3.3. Monte Carlo modeling of exposure and burial durations

We considered both nuclides together to calculate the minimum total history (single period of exposure followed by single period of burial) since initial exposure [or at least since erosional resetting of sufficient magnitude], by solving the following equations as in Bierman et al. (1999).

$$N_{Be} = \frac{P_{Be}}{\lambda_{Be}}[1 - \exp(-\lambda_{Be}t_e)]\exp(-\lambda_{Be}t_b) \quad (1)$$

$$N_{Al} = \frac{P_{Al}}{\lambda_{Al}}[1 - \exp(-\lambda_{Al}t_e)]\exp(-\lambda_{Al}t_b) \quad (2)$$

Equations were solved simultaneously to calculate the minimum total exposure duration (t_e) and minimum total burial duration (t_b), consistent with the measured ^{10}Be (N_{Be}) and ^{26}Al (N_{Al}) concentrations (Table 2). Here, P_{Be} and P_{Al} are the time-averaged, site-specific production rates, and λ_{Be} and λ_{Al} are the decay constants for ^{10}Be and ^{26}Al, respectively. Site-specific production rates were determined by scaling a conservative sea level, high latitude (SLHL) global production rate for ^{10}Be (4.0 ± 0.4 ^{10}Be atoms g^{-1} yr^{-1}, 1σ), based on the calibration datasets presented in Borchers et al. (2016), with a corresponding ^{26}Al production rate of 27.0 ± 2.6 ^{26}Al atoms g^{-1} yr^{-1} (assuming an $^{26}Al/^{10}Be$ production ratio of 6.75; Nishiizumi et al., 2007), to each site using the time-dependent nuclide-specific scaling of Lifton et al. (2014) (LSD framework). The ^{10}Be production rate is derived from pooled "primary" and "secondary" calibration site measurements used in the CRONUS-Earth project (Borchers et al., 2016; Phillips et al., 2016), which have been recalibrated using locally executable code based on the CRONUS online calculator of Balco et al. (2008), and the calibration code of Balco et al. (2009), updated to incorporate the LSD scaling, atmospheric, and geomagnetic frameworks (Lifton et al., 2014). We used our calibration code, as opposed to that of Borchers et al. (2016), since it shares a common base with other codes used in this study, allowing for internally consistent calculations throughout our analysis. Although this production rate is statistically identical to the Arctic ^{10}Be production rate of Young et al. (2013) (3.96 ± 0.07 atoms g^{-1} yr^{-1}), we favor the former because it includes uncertainties due to site-specific factors, such as potential variations in atmospheric structure.

The paired equations were solved for each sample using the non-linear least squares algorithm (*fsolve*) in MATLAB®, and uncertainties estimated by a 1000 iteration Monte Carlo simulation (Supplemental Material; Balco et al., 2014). Minimum exposure and burial durations, and the uncertainties associated with each, were calculated as the arithmetic mean and standard deviation of the 1000 simulations. Reported uncertainties are measurement errors

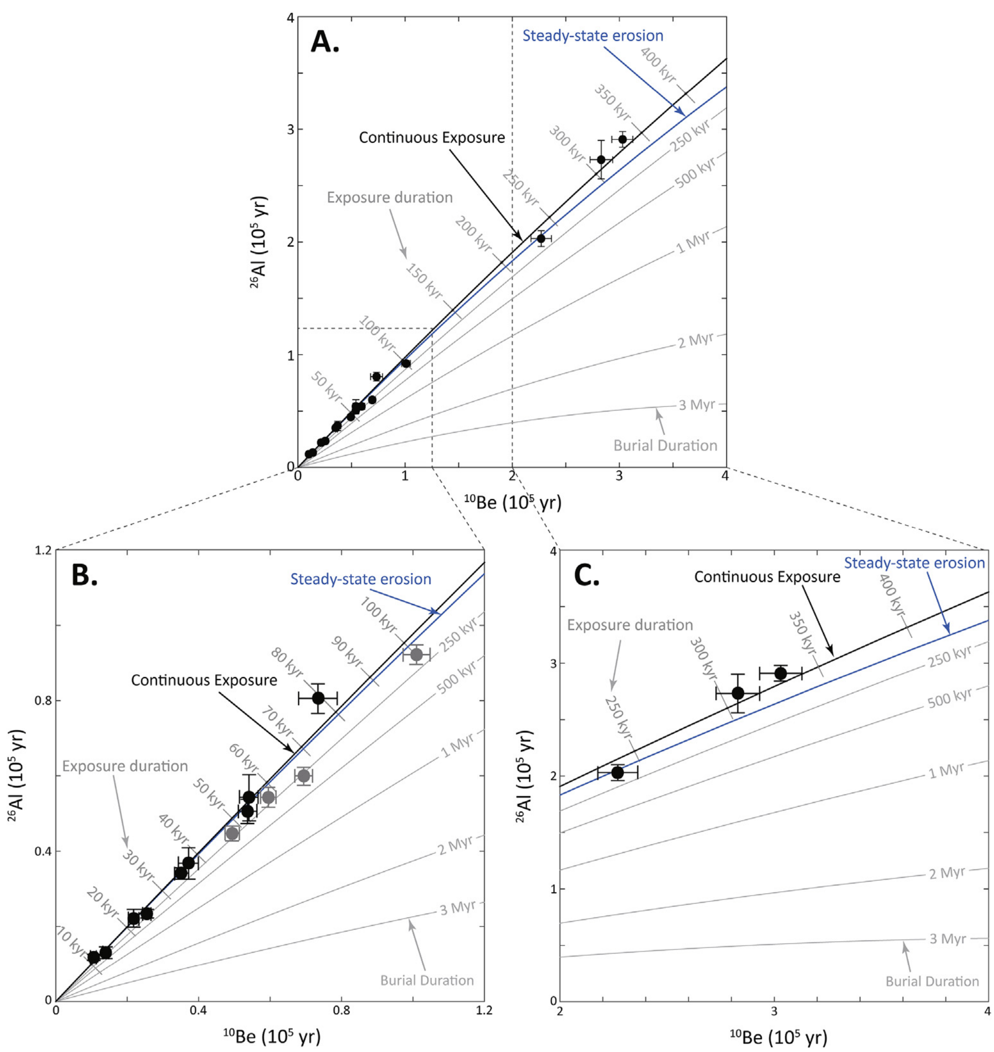

Fig. 4. ^{10}Be-^{26}Al two-isotope plot for the Uummannaq region (A). We use a split axis to display the full detail of samples over the observed range of ages (B and C). Analytical results are normalized to its corresponding present-day site production rate. The horizontal and vertical axes thus each have units in years. Analytical uncertainties are plotted at the 2σ level. Analytical uncertainties are shown as 2σ error bars. Error bars not visible are smaller than the marker size. Solid black line represents continuous exposure; solid blue line represents steady-state erosion; solid gray lines represent burial durations. Note most samples plot along or within 2σ of the continuous exposure line (black dots) except four samples that plot below in the area of significant burial (gray dots). See Table 2 for details. (For interpretation of the references to colour in this figure legend, the reader is referred to the web version of this article.)

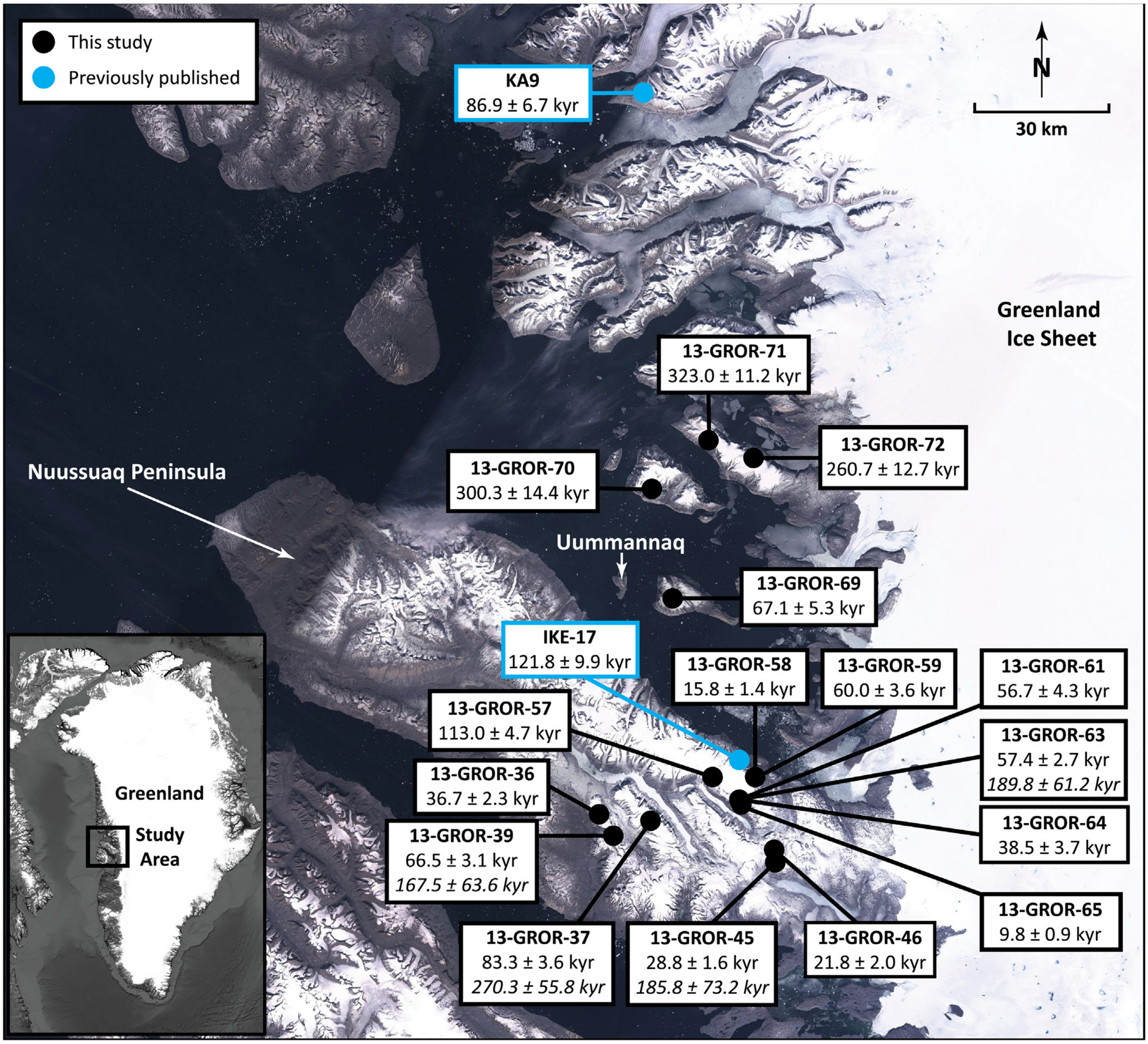

Fig. 5. Minimum exposure and burial duration estimates from Monte Carlo simulations for the Uummannaq region (black dots), showing sample locations relative to central-west Greenland (inset). IKE-17 and KA5 recalculated from Roberts et al. (2013) and Lane et al. (2014), respectively. Exposure and burial durations are shown as plain and italic text in each box, respectively. Exposure/burial durations calculated as the arithmetic mean and standard deviation of 1000 model simulations, shown here at the 1σ level. Samples with no burial duration displayed represent samples with nuclide abundances at or close to continuous exposure (i.e., zero burial) (satellite image source: ASTER and SPOT-5 DEM's – Howat et al., 2014).

only. We do not consider production rate uncertainties here, as those affect all samples similarly and do not change the relationships among the results (e.g., Balco, 2011). Although these sample histories are simplified single-exposure, single-burial period histories, they provide robust information about the minimum sample history. More complicated, and perhaps realistic, histories that follow glacial (burial)-interglacial (exposure) cycles, would yield longer total sample histories, but choosing exposure/burial durations is more subjective and adds uncertainty, and such results are not central to our conclusions. Total sample histories are the sum of the exposure and burial durations with attendant uncertainties assuming linear propagation of errors from the exposure and burial durations, respectively. Samples with indeterminate burial durations are displayed as dashes in Table 2 (e.g., zero burial or negative burial durations, with $^{26}Al/^{10}Be$ ratios exceeding the canonical ratio 6.75 of Nishiizumi et al., 2007), and represent samples with nuclide abundances consistent with continuous exposure. No correction was made for potential Holocene exposure/burial as these samples were generally collected within several m of ice cap margins rapidly retreating from their local Little Ice Age extents. Holocene exposure is certainly possible, and perhaps likely, but assumed exposure and burial durations would be speculative without additional data.

4. Results

Resulting exposure histories are summarized in Table 2. Resultant probability distributions for the Monte Carlo simulations are presented in the Supplementary Material. In Figs. 4 and 5 we

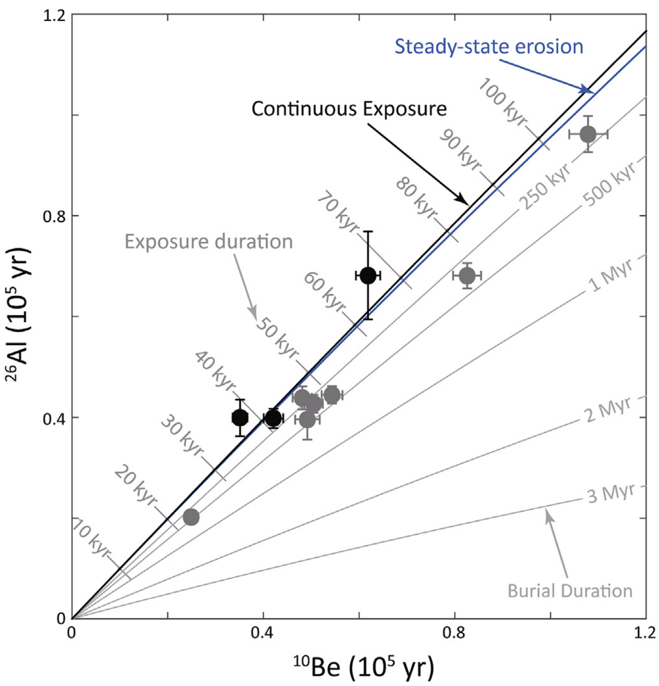

Fig. 6. ^{10}Be-^{26}Al two-isotope plot for the Sukkertoppen region. Analytical uncertainties are shown as 2σ error bars. Error bars not visible are smaller than the marker size. Solid black line represents continuous exposure; solid blue line represents steady-state erosion; solid gray lines represent burial durations. Note most samples plot below the continuous exposure line in the area of significant burial (gray dots), and only three samples have concentrations consistent with continuous exposure (black dots) at the 2σ level. See Table 2 for details. (For interpretation of the references to colour in this figure legend, the reader is referred to the web version of this article.)

graphically present the ^{10}Be and ^{26}Al concentration results on a two-isotope plot and the minimum exposure/burial durations on a satellite image, respectively, for the Uummannaq region. The same graphical representations for the Sukkertoppen region are presented in Figs. 6 and 7, respectively. The two-isotope plots are graphically presented following the format suggested by Balco and Rovey (2008) and Granger (2014) and in contrast to the more common paired-nuclide ratio versus concentration "banana" plot of Lal (1991). Sample concentrations displayed on the two-isotope plots are normalized to their corresponding present-day site production rate (Figs. 4 and 6). Unit analysis yields horizontal and vertical axes with units in years (atoms/g normalized by atoms/g/yr), although it should be noted that these years do not incorporate corrections for respective nuclide decay. In Figs. 4 and 6, uncertainties are shown at the 2σ level. While analytical uncertainty at the 1σ level would generally be considered adequate, we argue that the 2σ level is more robust.

Before proceeding further, it is important to define the concept of both a detectable burial signal. We argue that a burial duration less than the equivalent burial duration required for the ^{26}Al/^{10}Be ratio to decay to a value at least two-sigma less than the ^{26}Al/^{10}Be production ratio is not detectable and thus not geologically significant. Based on the mean uncertainty of the ^{26}Al/^{10}Be ratios presented here, the average minimum detectable burial signal is equivalent to 173 kyr. Detection limits of burial for each sample are included in Table 2.

4.1. Uummannaq region

Paired measurements of ^{10}Be and ^{26}Al were made on 16 samples from the Uummannaq region (Tables 1 and 2). In general, most of the measured ^{26}Al/^{10}Be ratios are close to the production ratio of ca. 6.75. However, four samples are less than the production rate ratio at 2σ (Table 2) and plot below the lines of continuous exposure and steady-state erosion (Fig. 4). Measured concentrations yield minimum exposure durations between ca. 10 and ca. 300 kyr, and burial durations (with large uncertainties) between ca. 160 and ca. 270 kyr (Table 2). Combining exposure and burial durations yield minimum total histories between ca. 200 and ca. 350 ka (Table 2).

Results vary spatially in a complicated manner (Fig. 5). Twelve of the 16 samples have long exposure (between ca. 60 and ca. 300 kyr), and burial durations at undetectable levels (i.e., <173 kyr). In addition, the majority of samples on the Nuussuaq Peninsula have varying durations of exposure with no detectable burial, except for four samples located near the center of the peninsula.

4.2. Sukkertoppen region

In contrast, paired ^{10}Be and ^{26}Al concentration measurements on the 10 samples from the Sukkertoppen region yield minimum exposure durations between ca. 30 and ca. 125 kyr (Tables 1 and 2 and Fig. 7). Most of the measured ^{26}Al/^{10}Be ratios ($n = 7$) are less than the production ratio of ca. 6.75 (Table 2), plotting within the area of detectable burial on the two-isotope plot at 2σ (Fig. 6). For these seven samples, measured concentrations yield burial duration estimates between ca. 170 and ca. 400 kyr, but with large uncertainties (Table 2). These samples yield total histories between ca. 200 and ca. 500 ka (Table 2). The remaining three samples have ^{26}Al/^{10}Be ratios consistent with the production ratio, overlapping with the line of continuous exposure at 2σ (Fig. 6).

5. Discussion

Upland surfaces surrounding the Uummannaq and Sukkertoppen regions provide evidence that the evolution of the landscape and the history of the GIS along Greenland's western coastline vary due to differences in landscape character. Our results from the Uummannaq region reveal no significant long-term burial, consistent with previous findings (Roberts et al., 2013; Lane et al., 2014). Reconstructions of the Uummannaq Ice Stream profile at the LGM (Roberts et al., 2013; Lane et al., 2014), coupled with our findings here, suggest the possibility that high-elevation surfaces in the Uummannaq region may have remained as nunataks above the GIS surface for much of the middle and late Quaternary, possibly even during the LGM. If true, we speculate that the mechanism for preserving these nunataks may be major ice surface drawdown in the Uummannaq Ice Stream System (UISS). Conceivably, this could occur when major fjord glaciers draining the GIS encounter a marked reduction in basal shear stress at the land/marine transition, leading to high ice flux and a low-gradient ice surface profile. In fact, our three samples with the longest exposure (260–300 kyr), and yet no detectable burial, are from islands within the Uummannaq fjord system, consistent with ice sheet drawdown in the marine embayment.

Our results from the Sukkertoppen region suggest that parts of this terrain have been preserved through much of the middle and late Quaternary. In contrast to Uummannaq, burial is a significant component of the total landscape history around Sukkertoppen; samples exhibit a mean burial-to-total-history ratio of 0.79 ± 0.11 (1σ). This is comparable to the findings of Corbett et al. (2013) in Upernavik, ca. 600 km to the north, where samples yield a mean ratio of burial-to-total-history of 0.76 ± 0.08 (1σ). However, on average, high-elevation surfaces from Upernavik have longer minimum exposure durations, burial durations, and total histories than the sampled surfaces in Sukkertoppen (recalculated from Corbett et al., 2013). In contrast, total histories on Cumberland

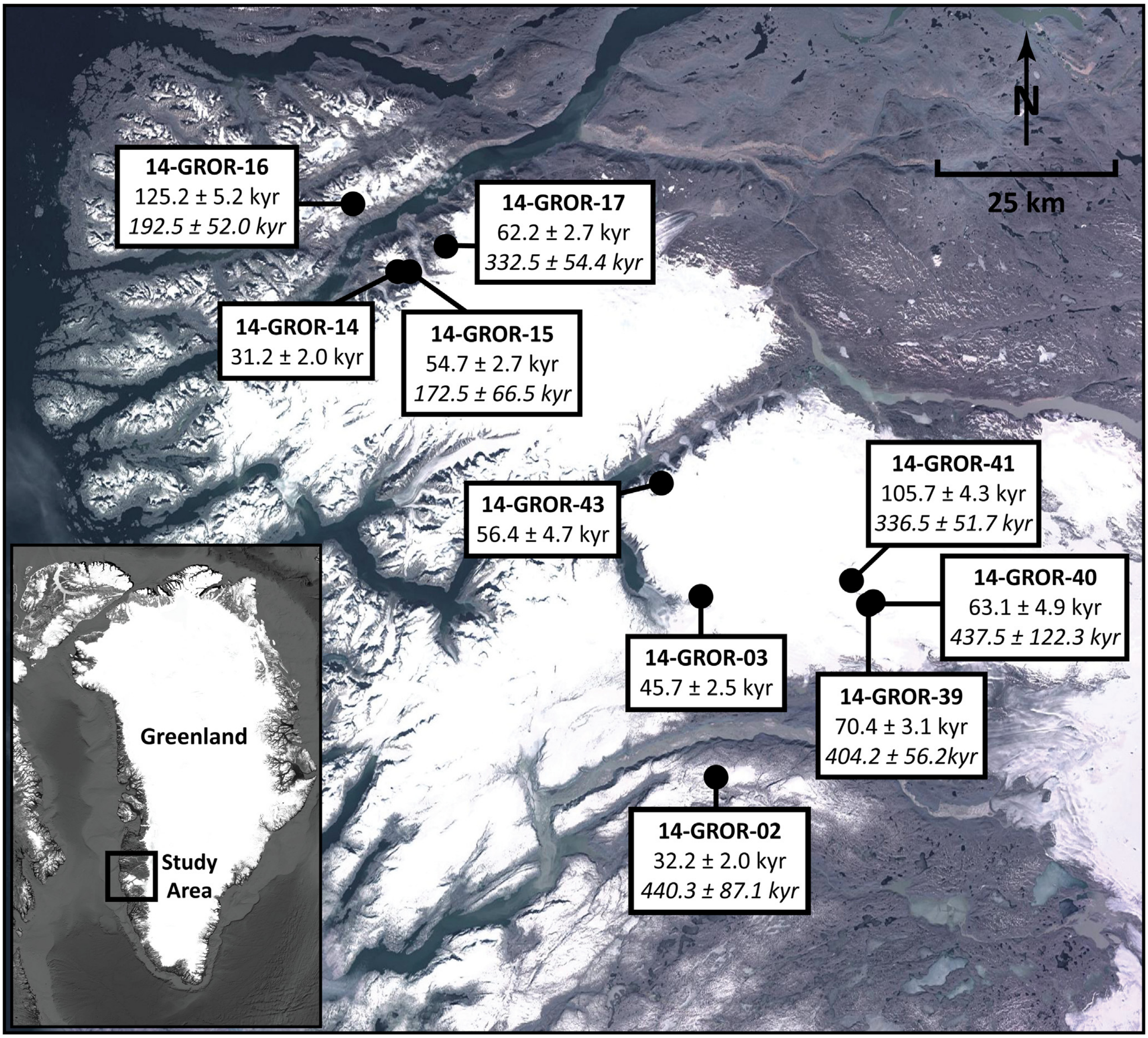

Fig. 7. Minimum exposure and burial duration estimates from Monte Carlo simulations for the Sukkertoppen region, showing sample locations relative to southwest Greenland (inset). Exposure and burial durations are shown as plain and italic text in each box, respectively (1σ). Exposure/burial durations are calculated as for the Uummannaq sites (satellite image source: ASTER and SPOT-5 DEM's – Howat et al., 2014).

Peninsula, Baffin Island (ca. 600 km to the west), are almost twice those of the Upernavik and Sukkertoppen regions (ca. 1 Myr) (recalculated from Bierman et al., 1999). Still, the Bierman et al. (1999) samples indicate a mean ratio of burial to total history of 0.87 ± 0.02 (1σ) – generally consistent with the western Greenland terrestrial fringe burial fraction results. Our data further support the suggestion of Corbett et al. (2013) that the value of ca. 0.8 for burial/total history may represent the fraction of time during late Quaternary glacial-interglacial cycles characterized by expanded ice volume around Baffin Bay.

Results from our two study regions – absence of burial in the embayment setting and significant burial within the wide terrestrial fringe – suggest more broadly that the Quaternary glacial history of terrestrial fringe settings may be different than those of marine embayment settings. Most of our data from the Sukkertoppen region (terrestrial fringe setting) are consistent with the interpretation that this landscape has been buried for long durations by cold-based ice that performed little to no erosion. In contrast, the majority of the dataset from the Uummannaq region (marine embayment setting) indicates long exposure durations with little to no burial – consistent with an interpretation that those surfaces have been apparently continuously exposed through much of the latter Quaternary. This finding from the Uummannaq region of such surface antiquity with no detectable burial is unique in Arctic settings (Gjermundsen et al., 2015), and contrasts with data from other sites thus far studied surrounding Baffin Bay (e.g., Corbett et al., 2013, 2016; Bierman et al., 1999). On the other hand, if future work near large and deep marine embayments yields similar results, these regions may be the most likely to contain high-elevation nunatak areas that remain continuously exposed during maximum glacial stages.

To illustrate the uniqueness of the Uummannaq region in Arctic

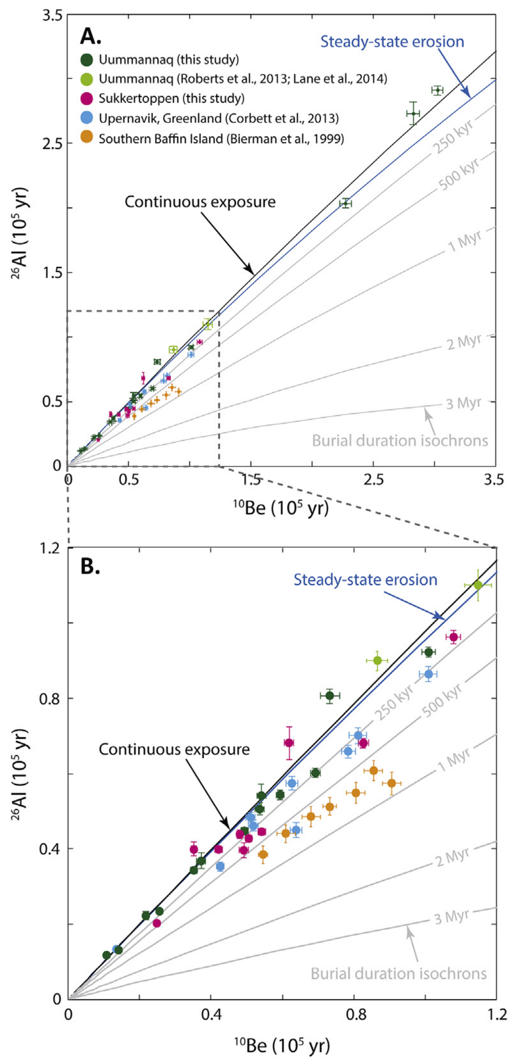

Fig. 8. ^{10}Be-^{26}Al two-isotope plots for available data from areas surrounding Baffin Bay (including samples presented here). Analytical uncertainties at the 2σ level shown. Error bars not visible are smaller than the marker size. Samples from the Uummannaq area are unique in this combined dataset; consistent with an interpretation of continuous exposure in a region usually dominated by burial by glacial ice.

settings, we plot our data on a two-isotope plot against available paired measurements from western Greenland for Uummannaq (Roberts et al., 2013; Lane et al., 2014) and Upernavik (Corbett et al., 2013), and with representative data from eastern Baffin Island (Bierman et al., 1999) (Fig. 8). Following Corbett et al. (2013), we only consider bedrock samples at elevations >600 m asl, and have recalculated all results with our model. The apparent continuous exposure of samples from the marine embayment setting of Uummannaq is clearly distinct from the burial-dominated landscape history for samples from high-elevation uplands surrounding Baffin Bay. However, in a recent study from distal locations in eastern Baffin Island, Margreth et al. (2016) found that some samples show dominance of exposure, not burial. In any case, although most samples from the Uummannaq region have nuclide concentrations consistent with an interpretation of continuous exposure, measurement uncertainties do not allow us to rule out the possibility of burial by cold-based ice for durations only tens-of-thousands of years (Balco et al., 2014).

Curiously, the samples from central Uummannaq with the longest exposure, yet no detectable burial, were collected from surfaces that had just emerged (within the past decade) from receding ice cap margins. This indicates that these sites have been buried by local ice caps during the Holocene, yet they apparently escaped long-term burial by the GIS during glacial periods, perhaps even the LGM. We find it surprising that many of these sites are exposed during glacial periods of the latter Quaternary, yet were buried during at least portions of the Holocene interglacial. We speculate that this may reflect differences in precipitation patterns on inter-fjord plateaus in the Uummannaq area, between major glacial periods and the late Holocene. For example, during glacial periods, when the uplands were ice-sheet free, they may have been starved of moisture due to extensive sea ice cover in Baffin Bay. In contrast, precipitation rates may have been much higher during the Holocene, and allowed ice to accumulate on the inter-fjord uplands. It is also possible that these sites may have been buried beneath glacial ice during both glacial and interglacial periods that was not sufficiently thick to block cosmogenic nuclide production (e.g., on the order of 50–100 m).

6. Conclusions

We present cumulative histories of exposure and burial for upland sites surrounding the marine embayment setting of Uummannaq and the terrestrial fringe setting of Sukkertoppen along the western margin of Greenland. Paired cosmogenic nuclide calculations (^{10}Be, ^{26}Al) from these two landscape types yielded contrasting histories for the latter Quaternary in Monte Carlo-based exposure and burial calculations. Surfaces in the Uummannaq region exhibit total minimum histories consistent with nearly continuous exposure; perhaps with some burial beneath ice cover thin enough to allow continued significant cosmogenic nuclide production through multiple glacial-interglacial cycles. This suggests that surfaces in this region may have remained as nunataks during glacial cycles, perhaps even during the LGM, likely due to significant ice drawdown in the UISS. Conversely, surfaces in the Sukkertoppen landscape exhibit ^{10}Be and ^{26}Al concentrations consistent with preservation under minimally-erosive, cold-based ice through much of the Quaternary.

Acknowledgments

This research was supported by a Purdue Rare Isotope Measurement Laboratory (PRIME Lab) seed grant and a Purdue Climate Change Research Center (PCCRC) Lynn Fellowship to C. Beel. This research was also supported by a National Science Foundation (NSF) grant ARC-1204096 to N. Lifton and ARC-1204005 to J. Briner. We would like to thank Gifford Miller, Ole Bennike, Avy Schweinsberg, Sam Kelley, Alia Lesnek, Christina Ciarametaro and Sandra Cronauer for assistance in the field, and to CH2M Hill Polar Services for logistical support on Greenland.

Appendix A. Supplementary data

Supplementary data related to this article can be found at http://dx.doi.org/10.1016/j.quascirev.2016.05.033.

References

Balco, G., Rovey, C., 2008. An isochron method for cosmogenic-nuclide dating of buried soils and sediments. Am. J. Sci. 308, 1083–1114.
Balco, G., Stone, J.O., Lifton, N.A., Dunai, T.J., 2008. A complete and easily accessible means of calculating surface exposure ages or erosion rates from ^{10}Be and ^{26}Al measurements. Quat. Geochronol. 3, 174–195.
Balco, G., Briner, J., Finkel, R.C., Rayburn, J.A., Ridge, J.C., Schaefer, J.M., 2009. Regional beryllium-10 production rate calibration for late-glacial northeastern North America. Quat. Geochronol. 4, 93–107.
Balco, G., 2011. Contributions and unrealized potential contributions of cosmogenic-

nuclide exposure dating to glacier chronology, 1990–2010. Quat. Sci. Rev. 30, 3–27.
Balco, G., Stone, J.O.H., Sliwinski, M.G., Todd, C., 2014. Features of the glacial history of the Transantarctic Mountains inferred from cosmogenic ^{26}Al, ^{10}Be and ^{21}Ne concentrations in bedrock surfaces. Antarct. Sci. 26 (6), 708–723.
Bierman, P.R., Marsella, K.A., Patterson, C., Davis, P.T., Caffee, M., 1999. Mid-Pleistocene cosmogenic minimum-age limits for pre-Wisconsinan glacial surfaces in southwestern Minnesota and southern Baffin Island: a multiple nuclide approach. Geomorphology 27, 25–39.
Borchers, B., Marrero, S., Balco, G., Caffee, M., Goehring, B., Lifton, N., Nishiizumi, K., Phillips, F., Schaefer, J., Stone, J., 2016. Geological calibration of spallation production rates in the CRONUS-Earth project. Quat. Geochronol. http://dx.doi.org/10.1016/j.quageo.2015.01.009.
Briner, J.P., Miller, G.H., Davis, P.T., Finkel, R.C., 2006. Cosmogenic radionuclides from fjord landscapes support differential erosion by overriding ice sheets. GSA Bull. 118 (3/4), 406–420. Data Repository item 2006046.
Briner, J.P., Lifton, N.A., Miller, G.H., Refsnider, K., Anderson, R., Finkel, R., 2014. Using *in situ* cosmogenic ^{10}Be, ^{14}C, and ^{26}Al to decipher the history of polythermal ice sheets on Baffin Island, Arctic Canada. Quat. Geochronol. 19, 4–13.
Chalmers, J.A., Pulvertaft, T.C.R., Marcussen, C., Pedersen, A.K., 1999. New insight into the structure of the Nuussuaq Basin, central west Greenland. Mar. Petroleum Geol. 16, 197–224.
Chmeleff, J., Blanckenburg von, F., Kossert, K., Jakob, D., 2010. Determination of the ^{10}Be half-life by multicollector ICP-MS and liquid scintillation counting. Nucl. Instrum. Methods Phys. Res. Sect. B 268, 192–199.
Corbett, L.B., Young, N.E., Bierman, P.R., Briner, J.P., Neumann, T.A., Rood, D.H., Graly, J.A., 2011. Paired bedrock and boulder ^{10}Be concentrations resulting from early Holocene ice retreat near Jakobshavn Isfjord, western Greenland. Quat. Sci. Rev. 30, 1739–1749.
Corbett, L.B., Bierman, P.R., Grady, J.A., Neumann, T.A., Rood, D.H., 2013. Constraining landscape history and glacial erosivity using paired cosmogenic nuclides in Upernavik, northwest Greenland. Geol. Soc. Am. Bull. 125 (9), 1539–1553.
Corbett, L.B., Bierman, P.R., Rood, D.H., 2016. Constraining multi-stage exposure-burial scenarios for boulders preserved beneath cold-based glacial ice in Thule, northwest Greenland. Earth Planet. Sci. Lett. 440, 147–157. http://dx.doi.org/10.1016/j.epsl.2016.02.004.
Davis, P.T., Briner, J.P., Coulthard, R.D., Finkel, R.W., Miller, G.H., 2006. Preservation of Arctic landscapes overridden by cold-based ice sheets. Quat. Res. 65, 156–163.
Fabel, D., Stroeven, A.P., Harbor, J., Kleman, J., Elmore, D., Fink, D., 2002. Landscape preservation under Fennoscandian ice sheets determined from in situ produced ^{10}Be and ^{26}Al. Earth Planet. Sci. Lett. 201, 397–406.
Gosse, J., Grant, D., Klein, J., Lawn, B., 1995. Cosmogenic ^{10}Be and ^{26}Al constraints on weathering zone genesis, ice cap basal conditions, and Long Range Mountain (Newfoundland) glacial history. In: Proceedings of the Canadian Quaternary Association–Canadian Geomorphology Research Group (CANQUA-CGRC) Conference Abstracts. Memorial University, Saint Johns, Newfoundland v. CA19.
Granger, D.E., 2014. Cosmogenic nuclide burial dating in archaeology and paleoanthropology. In: Cerling, T.E. (Ed.), Archaeology and Anthropology, pp. 81–97. Volume 14 in Turekian, K.K., and HollandH.D. (Eds.), Treatise on Geochemistry, Elsevier-Pergamon, Oxford.
Gjermundsen, E.F., Briner, J.P., Akçar, N., Kubik, P.W., Salvigsen, O., Hormes, A., 2015. Minimal erosion of Arctic alpine topography during late Quaternary glaciation. Nat. Geosci. 8, 789–793.
Henriksen, N., 2008. Geological History of Greenland – Four Billion Years of Earth Evolution. Geological Survey of Denmark and Greenland (GEUS), Copenhagen, p. 272.
Howat, I.M., Negrete, A., Smith, B.E., 2014. The Greenland Ice Mapping Project (GIMP) land classification and surface elevation datasets. Cryosphere 8, 1509–1518.
Kelly, M.A., Lowell, T.V., 2009. Fluctuations of local glaciers in Greenland during the latest Pleistocene and Holocene time. Quat. Sci. Rev. 28, 2088–2106.
Kohl, C.P., Nishiizumi, K., 1992. Chemical isolation of quartz for measurement of *in-situ*-produced cosmogenic nuclides. Geochem. Cosmochim. Acta 56, 3583–3587.
Korschinek, G., Bergmaier, A., Faestermann, T., Gerstmann, U.C., Knie, K., Rugel, G., Wallner, A., Dillmann, I., Dollinger, G., Gostomski, C.L.V., Kossert, K., Maiti, M., Poutivtsev, M., Remmert, A., 2010. A new value for the half-life of ^{10}Be by Heavy-Ion Elastic Recoil Detection and liquid scintillation counting. Nucl. Instrum. Methods Phys. Res. B 268, 187–191.
Lal, D., 1991. Cosmic ray labeling of erosion surfaces: *in situ* nuclide production rates and erosion models. Earth Planet. Sci. Lett. 104, 424–439.
Lane, T.P., Roberts, D.H., Rea, B.R., Cofaigh, C.Ó., Vieli, A., Rodés, A., 2014. Controls upon the last glacial maximum deglaciation of the northern Uummannaq ice stream system, west Greenland. Quat. Sci. Rev. 92, 324–344.
Lifton, N.A., Sato, T., Dunai, T.J., 2014. Scaling *in situ* cosmogenic nuclide production rates using analytical approximations to atmospheric cosmic-ray fluxes. Earth Planet. Sci. Lett. 386, 149–160.
Lowell, T.V., Hall, B.L., Kelly, M.A., Bennike, O., Lusas, A.R., Honsaker, W., Smith, C.A., Levy, L.B., Travis, S., Denton, G.H., 2013. Late Holocene expansion of istorvet ice cap, liverpool land, east Greenland. Quat. Sci. Rev. 63, 128–140.
Margreth, A., Gosse, J.C., Dyke, A.S., 2016. Quantification of subaerial and episodic subglacial erosion rates on high latitude upland plateaus: Cumberland Peninsula, Baffin Island, Arctic Canada. Quat. Sci. Rev. 133, 108–129.
Miller, G.H., Lehman, S.J., Refsnider, K.A., Southon, J.R., Zhong, Y., 2013a. Unprecedented recent summer warmth in Arctic Canada. Geophys. Res. Lett. 40, 5745–5751.
Miller, G.H., Briner, J.P., Refsnider, K.A., Lehman, S.J., Geirsdóttir, A., Larsen, D.J., Southon, J.R., 2013b. Substantial agreement on the timing and magnitude of Late Holocene ice cap expansion between East Greenland and the Eastern Canadian Arctic: a commentary on Lowell et al., 2013. Quat. Sci. Rev. 77, 239–245.
Nishiizumi, K., 2004. Preparation of ^{26}Al AMS standards. Nucl. Instrum. Methods Phys. Res. Sect. B 223, 388–392.
Nishiizumi, K., Imamura, M., Caffee, M., Southon, J., Finkel, R.C., Mcaninch, J., 2007. Absolute calibration of ^{10}Be AMS standards. Nucl. Instrum. Methods Phys. Res. Sect. B Beam Interact. Mater. Atoms 258, 403–413.
Ochs, M., Ivy-Ochs, S., 1997. The chemical behavior of Be, Al, Fe, Ca and Mg during AMS target preparation from terrestrial silicates modeled with chemical speciation calculations. Nucl. Instrum. Methods Phys. Res. Sect. B 123, 235–240.
Phillips, F.M., Argento, D.C., Balco, G., Caffee, M.W., Clem, J., Dunai, T.J., Finkel, R., Goehring, B., Gosse, J.C., Hudson, A.M., Jull, A.J.T., Kelly, M.A., Kurz, M., Lal, D., Lifton, N., Marrero, S.M., Nishiizumi, K., Reedy, R.C., Schaefer, J., Stone, J.O.H., Swanson, T., Zreda, M.G., 2016. The CRONUS-Earth Project: a synthesis. Quat. Geochronol. 31, 119–154.
Roberts, D.H., Long, A.J., Schnabel, C., Freeman, S., Simpson, M.J.R., 2008. The deglacial history of southeast sector of the Greenland ice sheet during the last glacial maximum. Quat. Sci. Rev. 27, 1505–1516.
Roberts, D.H., Long, A.J., Schnabel, C., Davies, B.J., Xu, S., Simpson, M.J.R., Huybrechts, P., 2009. Ice sheet extent and early deglacial history of the southwestern sector of the Greenland Ice Sheet. Quat. Sci. Rev. 28, 2760–2773.
Roberts, D.H., Long, A.J., Davies, B.J., Simpson, M.J.R., Schnabel, C., 2010. Ice stream influence on west Greenland ice sheet dynamics during the last glacial maximum. J. Quat. Sci. 25 (6), 850–864.
Roberts, D.H., Rea, B.R., Lane, T.P., Schanbel, C., Rodés, A., 2013. New constraints on Greenland ice sheet dynamics during the last glacial cycle: evidence from the Uummannaq ice stream system. J. Geophys. Res. Earth Surf. 118, 1–23.
Seo, K.W., Waliser, D.E., Lee, C.K., Tian, B., Scambos, T., Kim, B.M., van Angelen, J.H., van den Broeke, M.R., 2015. Accelerated mass loss from Greenland ice sheet: links to atmospheric circulation in the North Atlantic. Glob. Planet. Change 128, 61–71.
Stroeven, A.P., Fabel, D., Hätterstrand, C., Harbor, J., 2002. A relict landscape in the center of Fennoscandian glaciation: cosmogenic radionuclide evidence of tors preserved through multiple glacial cycles. Geomorphology 44, 145–154.
Weidick, A., Bøggild, C.E., Knudsen, N.T., 1992. Glacier inventory and atlas of west Greenland. Grønl. Geol. Unders. Rapp. 158, 194.
Young, N.E., Schaefer, J.M., Briner, J.P., Goehring, B.M., 2013. A ^{10}Be production-rate calibration for the Arctic. J. Quat. Sci. 28 (5), 515–526.